Journal of Geophysical Research: Biogeosciences

RESEARCH ARTICLE
10.1029/2018JG004536

Ecosystem-Scale Measurements of Methyl Halide Fluxes From a Brackish Tidal Marsh Invaded With Perennial Pepperweed (*Lepidium latifolium*)

M. J. Deventer[1,2], Y. Jiao[1], S. H. Knox[3], F. Anderson[4], M. C. Ferner[5], J. A. Lewis[5], and R. C. Rhew[1]

[1]Department of Geography, University of California, Berkeley, CA, USA, [2]Now at Department of Soil, Water and Climate, University of Minnesota, Twin Cities, St. Paul, MN, USA, [3]Department of Earth System Science, Stanford University, Stanford, CA, USA, [4]California Water Science Center, U.S. Geological Survey, Sacramento, CA, USA, [5]San Francisco Bay National Estuarine Research Reserve, San Francisco State University, Tiburon, CA, USA

Key Points:
- These are the first ecosystem-scale flux measurements of methyl halides using the relaxed eddy accumulation method
- Methyl halide emissions follow a seasonal pattern, controlled by temperature and the halophyte growth cycle, with episodic spikes during heat waves
- The invasive perennial pepperweed (*Lepidium latifolium*) contributes significantly to the overall emissions

Supporting Information:
- Supporting Information S1

Correspondence to:
M. J. Deventer,
deventer@umn.edu

Citation:
Deventer, M. J., Jiao, Y., Knox, S. H., Anderson, F., Ferner, M. C., Lewis, J. A., & Rhew, R. C. (2018). Ecosystem-scale measurements of methyl halide fluxes from a brackish tidal marsh invaded with perennial pepperweed (*Lepidium latifolium*). *Journal of Geophysical Research: Biogeosciences*, *123*, 2104–2120. https://doi.org/10.1029/2018JG004536

Received 12 APR 2018
Accepted 5 JUN 2018
Accepted article online 15 JUN 2018
Published online 13 JUL 2018

Abstract Natural methyl chloride (CH_3Cl) and methyl bromide (CH_3Br) emissions from coastal marsh ecosystems may constitute a significant proportion of stratospheric chlorine and bromine, which catalyze ozone depletion. Current inventories involve substantial uncertainties associated with upscaling plot-scale footprints (i.e., $\leq$1 m^2). Here we present net ecosystem flux measurements of methyl halides from a brackish tidal marsh on the west coast of the United States between April 2016 and June 2017 using the relaxed eddy accumulation method. The measurement footprint encompasses a large part of the studied tidal marsh, including roughly 20 vascular plant species, open water, and soil surfaces. On the annual scale, ecosystem methyl halide emissions showed the strongest relationships to temperature and the growth cycle of halophyte vegetation, whereas on diurnal time scales, fluxes correlated the most with evapotranspiration. The maximum seasonal emissions occurred during the flowering season of *Lepidium latifolium* (perennial pepperweed), one of the most abundant halophytes on site. The maximum hourly emissions of 111 μg $CH_3Cl \cdot m^{-2} \cdot hr^{-1}$ and 38 μg $CH_3Br \cdot m^{-2} \cdot hr^{-1}$ were observed during a heat wave in early June. Annually integrated emissions were 135 mg/m^2 for CH_3Cl and 21 mg/m^2 for CH_3Br, scaling up to 621 and 96 kg over the entire marsh. We provide a global salt marsh emission inventory that takes into account the spatial distribution of salt marshes in different climate zones, yielding a global salt marsh source of 31 Gg/year CH_3Cl (range: 10 to 77) and 3 Gg/year CH_3Br (range: 1 to 8).

1. Introduction

Methyl chloride (CH_3Cl) and methyl bromide (CH_3Br) are major carriers of chlorine (16% of total) and bromine (50% of total) into the stratosphere, and consequently, both compounds are classified as ozone depleting substances (Carpenter et al., 2014). Methyl iodide (CH_3I), a much shorter lived species, is the main organic volatile transporting iodine from the oceans and the biosphere into the troposphere, where it has important implications for oxidative capacity and ozone chemistry (Carpenter et al., 2014; Stemmler et al., 2013). While global mean surface concentrations of CH_3Br have declined owing to the phase-out of this compound due to implementation of the Montreal Protocol, concentrations of CH_3Cl have stayed essentially constant since 2008 (Carpenter et al., 2014). Long-term trends and source budgeting of CH_3I are highly uncertain but interannual CH_3I variation correlated with global sea surface temperatures, hinting toward a dominant ocean source (Carpenter et al., 2014; Yokouchi et al., 2012).

Despite extensive terrestrial field observations of CH_3Cl and CH_3Br, global budgets of both compounds remain unbalanced, with sinks outweighing identified sources. Both compounds have anthropogenic and shared natural sources. Nonagricultural and nonindustrial emissions now constitute the larger share of both methyl halides at ≈80% for CH_3Br and ~90% for CH_3Cl. Biomass burning and oceanic emissions are the two largest sources for both methyl halides, summing up to ≈40% for CH_3Br and ≈30% for CH_3Cl (Carpenter et al., 2014; Hu et al., 2010). Large uncertainty exists about the contribution from individual terrestrial sources, although several studies have identified a substantial CH_3Cl source (≥1.4 Tg/year or up to 20%) in the tropics, both from the canopy of tropical rain forests and from leaf litter decomposition (Blei et al., 2010; Gebhardt et al., 2008; Saito et al., 2008; Yokouchi et al., 2002, 2007). In contrast, tropical methyl bromide emissions have not been identified yet. For CH_3I, top-down and bottom-up models of global emissions vary by a factor of 2,

indicating that relevant sources and sinks might yet be unknown. Besides the dominant ocean source, estimates for coastal ecosystems vary from 5% to 50%, or 60 to 280 Gg/year (Butler et al., 2007; Jones et al., 2010).

Outside of the tropics, coastal salt marshes are emission hot spots for both compounds, emitting up to an estimated 5% and 17% of global CH_3Cl and CH_3Br emissions, respectively, which is also estimated to be up to 12 times larger than the global freshwater wetland source (Carpenter et al., 2014). Observations of natural salt marshes emissions have been conducted in North America (Khan et al., 2013; Manley et al., 2006; Rhew & Mazéas, 2010; Rhew et al., 2000, 2014), Europe (Blei et al., 2010; Dimmer et al., 2001; Drewer et al., 2006), and Oceania (Cox et al., 2004). Reported fluxes, however, have a large variability, spanning over 3 orders of magnitude for CH_3Cl and 2 orders of magnitude for CH_3Br. This variability was attributed to spatial inhomogeneity, diurnal and seasonal fluctuations, and most prominently to the species composition of halophilic vegetation. Under notably elevated atmospheric background concentrations (up to 100 times larger than typical observations for the Northern Hemisphere), net CH_3Cl uptake was reported for one studied marsh in China (Wang et al., 2006). Using stable isotope tracers, (Rhew & Mazéas, 2010) showed that salt marshes in California have simultaneous bidirectional fluxes, but gross production from halophytic plants outweighed gross consumption in anaerobic soils by factors of 5 to 10, leading to exclusively positive net fluxes.

In all of these studies, static flux chambers (FCs) were employed to quantify exchange fluxes, enclosing a small surface area (a 0.04 to 1 m^2 flux footprint) of salt marsh vegetation, with measurement sites distributed to either capture different inundation regimes (lower to higher marsh; Blei et al., 2010; Rhew et al., 2000) or to study a variety of monospecific vegetation stands (Khan et al., 2013; Manley et al., 2006; Rhew et al., 2014). Observed fluxes were highly variable, even when experiments were paired in time, location, or enclosed vegetation species. Upscaling from point observations to global salt marsh fluxes consequently leads to large uncertainties, as reflected by the wide range of values in the most recent global budget: 1.1–170 Gg CH_3Cl/year and 0.6–14 Gg CH_3Br/year (Carpenter et al., 2014).

To tackle this systematic experimental constraint, we employed Relaxed Eddy Accumulation (REA), a micrometeorological measurement technique developed for in situ flux measurements between the atmosphere and large source areas (Businger & Oncley, 1990). This study represents the first ecosystem scale net flux measurements for these methyl halides, and the nonintrusive sampling technique allows the study of relationships between methyl halide fluxes and environmental drivers without biases associated with disturbance. Concurrent FC experiments over selected halophyte-dominated vegetation stands were conducted to compare emissions to REA-derived fluxes. This allowed an assessment of the emission potential of perennial pepperweed (*Lepidium latifolium*), a halophyte of the mustard family (Brassicaceae). The Brassicaceae family is known to include large methyl halide emitters, for example, rapeseed (Gan et al., 1998; Mead et al., 2008). One of the more pervasive competitive effects of *L. latifolium* invasion includes induced changes in biogeochemical cycling and to soil properties, chemistry and processes (Blank & Young, 2002). In light of *L. latifolium's* aggressive invasiveness and its ability to displace native marsh species (Bossard et al., 2000; Tobias et al., 2016), we investigate the implications of its geographical expansion on methyl halide emissions from invaded terrestrial ecosystems.

2. Methods

2.1. Study Site

Measurements were taken between 14 April 2016 and 16 June 2017 at the Rush Ranch Open Space Preserve (latitude/longitude: 38.2004°N, 122.0265°W), a 4.6-km^2 brackish tidal marsh (i.e., an oligohaline/mesohaline hydrological regime resulting from mixing of freshwater (<0.03‰ salinity) and marine water (>0.5‰ salinity). Rush Ranch is part of Suisun Marsh, the largest extant tidal marsh in the San Francisco Estuary (CA, United States). The regional climate can be classified as Mediterranean with hot-dry summers (Köppen: Csa). Only 2 months (January and December) have long-term temperature averages less than 10 °C (based on reference period 1991–2017, data source: Travis Air Force Base *KSUU*). Highest reference temperature averages of 22.5 °C occur in July and August, with a mean annual temperature of 16 °C. Mean annual precipitation is 497 mm. Drought years (e.g., 2000, 2003, 2015, and 2016) have annual precipitation sums on the order of 250 mm, whereas in wet years (winter 2016–2017 was notably wet) annual precipitation can reach 800 mm. Based on long-term observations the year of 2016 was slightly warm (a + 1 °C anomaly in average daily low temperature and slightly wet (518 mm). The start of 2017 was extremely wet, accumulating

580 mm of precipitation in January and February alone. Average sediment organic matter content in the 20-cm topsoil layer is 18 to 43.9%, bulk densities range between 0.25 and 0.41 g/cm^3, and carbon sequestration rates are estimated to be 80 g · m^{-2} · a^{-1} (Callaway et al., 2012).

Based on vegetation monitoring transects conducted in both 2015 and 2016, the vascular plant species are (in order of spatial coverage) the following: *Salicornia pacifica*, *Schoenoplectus americanus*, *Atriplex prostrates*, *Calystegia sepium*, *Cuscuta salina*, *Apium graveolens*, *Jaumea carnosa*, *L. latifolium*, *Typha dominguensis*, *Cressa truxillensis*, *Distichlis spicata*, *Triglochin concinum*, *Juncus arcticus*, *Bromus hordeaceous*, *Frankenia salina*, *Symphiotrichum subulatum*, and *Lotus corniculatus* (NERRS: NOAA National Estuarine Research Reserve System, 2016). Out of these, three halophytes are known to be important sources for methyl halides: *S. pacifica* with a 69% spatial coverage (range 3% to 90%), *L. latifolium* with 12% coverage (range 5% to 75%) and *F. salina* with 3% coverage (range 2% to 10%). Species composition highly varied along microclimate and hydrology gradients. For example, the native *F. salina* (alkali heath) favors the drier regions of the upper marsh whereas *S. pacifica* (pickleweed) favors lower parts of the marsh. In a 2011 study, Whitcraft et al. (2011) found 27% of the current estuarine wetland-associated flora at Rush Ranch are exotic species, and several are highly invasive. The invasive halophyte *L. latifolium* (perennial pepperweed) is native to Eurasia and was first documented in 1930s (Bellue, 1936). At Rush Ranch it is found across a wide array of soil moisture gradients, competing both with *J. arcticus* rushes and sedges in the wetter areas and with grasses like *D. spicata* in the drier parts. At the study site, *L. latifolium* forms large monospecific stands, leading to a dense white flowering canopy at heights of 1.2 m typically starting in May. Plants reach seed maturation in June and July, changing the color of the canopy from a distinct white into a brown white. From late September onward, plants get increasingly woody and die back, creating a thick litter layer, which gradually gets decomposed throughout the winter months and March. New shoots emerge from rhizomes between March and April.

2.2. Sampling Design

Flux measurements were performed at three different spatial scales: (i) ecosystem-scale measurements from a flux tower using the REA technique, yielding flux footprints of ≈1,000 m^2, (ii) static FCs with footprints = 0.25 m^2, and (iii) laboratory incubation of soil cores with footprints = 0.002 m^2.

2.2.1. REA Flux Measurements

Tidal wetlands are home to many endangered species, both in flora and fauna, limiting site accessibility over extended times of the year. Similar to other micrometeorological measurement techniques, REA is a nonintrusive technique to quantify the net exchange fluxes of a large surface (e.g., a representative part of an ecosystem) and the atmosphere. The method is described in detail in Businger and Oncley (1990). In short, a surface-atmosphere exchange can be derived by measuring the difference of an atmospheric scalar in air moving from the surface toward the atmosphere (upward) versus air moving from the atmosphere toward the surface (downward). Ambient air is conditionally sampled and accumulated into an up and down reservoir based on real-time measurements of the vertical wind component using sonic anemometry:

$$F = b\,\sigma w\left(\overline{c^{+}} - \overline{c^{-}}\right) \tag{1}$$

Here F is the REA flux, b is the dimensionless Businger-Oncley parameter, σw is the standard deviation of vertical wind speed (w), and $\overline{c^{+}}$ and $\overline{c^{-}}$ are the concentrations in the updraft and downdraft reservoirs indicated by the indices ($^{+}$) and ($^{-}$), respectively.

In this study, b was calculated based on concurrent eddy covariance (EC) measurements of a proxy scalar under the assumption of scalar similarity (Pattey et al., 1993). In this case, c in equation (2) is replaced by sonic temperature (T) measured in quasi-real time by the sonic anemometer. For each flux-averaging interval, b was dynamically calculated by rearranging equation (1) as follows:

$$b = \frac{\left(\overline{w'T'}\right)}{\sigma_w\left(\overline{T^{+}} - \overline{T^{-}}\right)}, \tag{2}$$

where $\left(\overline{w'T'}\right)$ is the covariance between instantaneous fluctuations of vertical wind (w') and temperature (T'), that is, the flux of sensible heat in EC formulation (Baldocchi et al., 1988). $\overline{T^{+}}$ and $\overline{T^{-}}$ are the mean temperatures during intervals of updraft and downdraft sampling. Following recommendations in Baker (2000) and similar to recent REA installments (Rhew et al., 2017; Riederer et al., 2014), we discarded sampling during

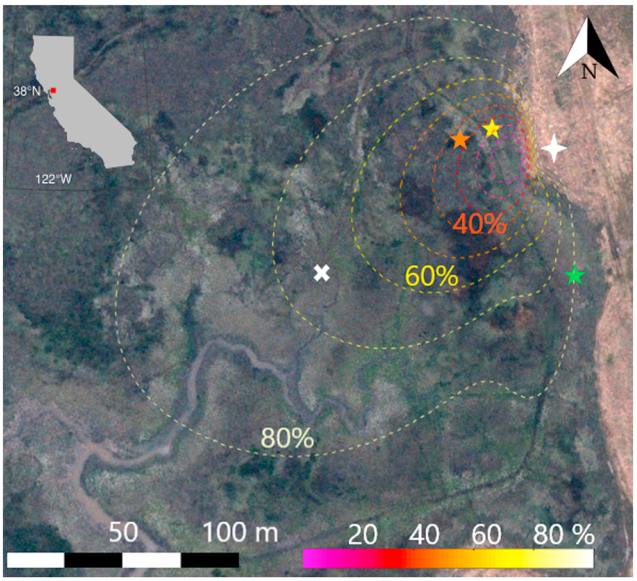

Figure 1. Aerial image (natural colors) of the Rush Ranch brackish marsh study site, with flux footprint climatology in dashed isolines colored according to the contribution heat map (from purple [10%] to white [80%]; Text S7). Star symbols mark the three flux chamber sites: *L. latifolium* (yellow and orange) and *F. salina* (green). Also shown are locations for the flux tower (white star) and the ancillary meteorological tower (white cross).

very low vertical wind speeds using a symmetrical deadband (w_0 = 0.6 σ_w) around the mean wind velocity for each flux-averaging interval, meaning that sampled air was only transferred into the reservoirs if $|w'| \geq w_0$.

The physical apparatus for conditional air sampling consists of two subsystems: (1) an air segregator with remote controlled fast-response valve switching between up-, down-, and neutral line, and (2) an air accumulation and reservoir system, equipped with vacuum pump for sample transfer and reservoir evacuation purposes (detailed plumbing diagram and flow description in supporting information Figure S1; the physical apparatus is described in detail in Rhew et al. (2017).

All instruments were installed on a 3 × 2 × 4 m (L × W × H) scaffolding tower (the U.S. Geological Survey-installed Rush Ranch main tower (Knox et al., 2018). The air segregator subsystem was mounted on a 1.2-m-long west facing metal extension at 2.20-m height. Air was drawn into the sampler through 75-cm polytetrafluoroethylene tubing (1/16″ inner diameter, EW06605-27, Cole Parmer, Vernon Hills, United States). The sample tube inlet was placed in close proximity (5-cm separation) to a sonic anemometer (Model 8100, R.M. Young, Traverse City, United States) at 3.1-m height. Fast measurements (5 Hz) of vertical wind speed were stored on a datalogger (CR-1000, Campbell Scientific Inc., Logan, United States), which controlled a fast-response solenoid valve (MP12-62 M, Bio-Chem Fluidics Inc., Boonton, United States). The reservoir subsystem 2 was placed on a tower platform at 1.6-m height. Ambient air was drawn through 1.5-m polytetrafluoroethylene tubing by a microdiaphragm pump (UNMP805, KNF Neuberger Inc., Trenton, United States) and accumulated in 10 l TEDLAR® bags (231-10, SKC Inc., Eighty Four, PA, United States) for 30-min time periods. One minute following the end of each accumulation interval, upsample and downsample were transferred into preevacuated stainless steel flasks (SilcoCan, Restek Corporation, Bellefonte, United States). Residual air was then evacuated to the atmosphere, by a vacuum pump.

Over the course of April 2016 to June 2017, 16 field outings were conducted at near monthly intervals to cover one full annual cycle of the tidal marsh ecosystem. Flux measurements typically started at 10 Pacific Standard Time (PST) and lasted through 16 PST. In this time frame, REA samples were taken every 30 min from the main tower setup. No REA flux measurements were taken in December and February because prevailing winds were from the east, causing the main tower's flux footprint (Kljun et al., 2015) to lie outside of the marsh.

2.2.2. Static FCs

In June 2016, two opaque aluminum chamber bases (10-cm height) with a square surface of 0.25 m^2 (50 cm × 50 cm) were inserted into the soil at 6 cm of depth. These *permanent* chambers were placed in a *L. latifolium*-dominated part of the marsh, roughly 5 m apart. A third chamber base was added in July on a *F. salina*-dominated patch at a drier part of the marsh, approximately 70 m south of the *L. latifolium* chambers, because of the known large emissions from this plant species (Manley et al., 2006; Rhew et al., 2000; Figure. 1). The top edges of the chamber bases were rimmed with a 2-cm-wide and 3-cm-deep channels, which, during incubations, were filled with deionized water to facilitate an airtight seal between the permanent chamber base and removable aluminum lid (either 46- or 92-cm height). Total enclosure volume during incubations was 0.28 m^3 for *L. latifolium* and 0.15 m^3 for *F. salina* chambers, respectively. Each chamber lid was equipped with two fans and a vent, which was temporarily opened to the atmosphere during sampling for pressure equilibration. Approximately 3 L of chamber air head space was sampled into preevacuated canisters (SilcoCan, Restek Corporation, Bellefonte, United States) at three equally spaced intervals, starting 1 min after the lid was placed. Fluxes were computed based on the increase of methyl halides in the chamber air over time:

$$F_{FC} = \frac{1}{A}\frac{dx}{dt}, \quad (3)$$

where F_{FC} is the FC flux, A is the enclosed surface area, x is the mole fraction of the studied gas in air, and t is time. Ambient air was also collected to determine the dilution effect from incoming air through the vent line (3 L per sample). Overall, chamber air leakage was $2\%_{vol}$ leading to flux corrections between 1% and 3%.

For each FC measurement, enclosed plant stems were counted and measured in height. A representative sample of vegetation was then harvested within a few meters from outside the FC footprint. Biomass was measured, both fresh (gfwt) and dried (gdwt) after 48 hr at 70 °C. Production rates were calculated by normalizing each FC flux observation by biomass. Starting June 2016, FC incubations for the two *L. laifolium*-dominated plots were conducted once per outing. Starting July 2016 we added a *F. salina*-dominated plot.

2.2.3. Soil Core Sampling and Incubations

A total of $n = 6$ soil cores (51-mm diameter and 6-cm depth) was collected on 27 April 2017 using a slide hammer (AMS, Inc., American Falls, United States) and stored inside an aluminum sheath at 5 °C. For incubations, the bottom of each sheath was first sealed using a stainless steel base plate, and then the entire core was placed into a 1.9-L Mason jar. At the start of each experiment, the jar was first flushed with ambient air and then sealed using a stainless steel lid with a Viton o-ring. Approximately 15 ml of headspace sample was drawn every 30 min, three times in total, starting at 1 min after sealing.

Soil core fluxes (F_{SC}) were calculated analogously to FCs using the increase in methyl halide concentration over time:

$$F_{SC} = \frac{1}{A_{core}} \frac{dx}{dt}, \tag{4}$$

with the soil core surface (A_{core}) and incubation time (t) in the denominator. If concentration gradients indicated net consumption, that is, negative $\frac{dx}{dt}$, the first-order uptake rate constant was determined as the slope of ln (x) versus time. Uptake rates were then normalized by multiplying the rate constant with seasonally averaged background concentrations of Northern Hemisphere air from 1998 to 2001 to be consistent with prior studies (e.g., Rhew & Mazéas, 2010). These were CH_3Br = 10.4 ppt, CH_3Cl = 535.7 ppt, and CH_3I = 1 ppt (Simmonds et al., 2004). Reported fluxes can be back calculated to rate constants, and these can be applied to different background concentrations, for example, to simulate uptake at different times or places.

2.2.4. Biomass Halide Content

Biomass samples were dried at 70 °C to constant weight and milled with a 60-mesh sieve. Approximately 0.5 g of milled biomass were boiled for 15 min in 40 ml of deionized water. The mixture was then centrifuged for 20 min (International Equipment Co., Needham, MA), and the supernatant was filtered through a ceramic Buchner funnel with a #5 Whatman filter and stored in Falcon tubes <0 °C prior to halide analysis. Each biomass sample was reextracted one additional times using the same methodology. Ion concentrations were analyzed using OrionTM electrodes (Thermo Electron Corporation, Waltham, MA). Each sample was analyzed at least twice on the same day, and calibration curves were conducted for every five samples measured. Plant halide concentrations were calculated as the cumulative mass of halides in the two consecutive extractions, normalized by the dry weight of biomass in units of grams halide per kilogram plant dry weight.

2.2.5. Air Analysis Instrumentation

Separation of different target species was performed using gas chromatography (GC) with cryogenic preconcentration. Separation and detection were performed on two separate systems, (a) a GC with mass spectrometry (GC-MS; Agilent 6890N/5973, Agilent Technologies, Santa Clara, United States) separating on a 1.4 um DB-VRX capillary column (J&W Scientific Inc., Folsom, United States; Rhew et al., 2007) and (b) a GC with oxygen-doped electron capture detection (GC-ECD; 5890SII, HP/Agilent Technologies, Santa Clara, United States) separating on a 22.5-m (0.53 mm I.D.) capillary Chrompack PoraPLOT Q column (Miller et al., 1998). For both systems, drifts in detection sensitivity were monitored through bracketed injections of a working standard (pressurized whole air collected from Trinidad Head, California, United States, calibrated at the Scripps Institution of Oceanography on the SIO-2008 scale) before and after sample sets (GC-MS) and before and after each individual run (GC-ECD).

Detector responses were checked for nonlinearity by injecting a series of working standards at different pressures, that is, along a known concentration gradient. Calibration curves were computed after each sampling set to correct data for nonlinear responses and daily instrumental drift. Peak integration and instrument automation were performed using GC-Werks software (www.gcwerks.com). REA samples were analyzed for CH_3Cl, CH_3Br and select on the GC-ECD system, whereas incubation samples were analyzed for CH_3Cl, CH_3Br, and

CH_3I, on the GC-MS. In a comparison study, air canisters from FC incubations were analyzed on both instruments on the same day. Resulting fluxes are within 1% (CH_3Cl) and 3.5% (CH_3Br) agreement. The GC-MS system has a much more linear response function and is hence better suited for large concentration gradients from incubation studies (here, in the order of 1 to 10 times atmospheric levels), whereas the GC-ECD system has superior analytical precision at atmospheric concentration levels and was hence used for REA samples. Consequently, CH_3I fluxes were only estimated for FC incubations. Blank studies were performed, and results are presented in supporting information (Text S1).

2.2.6. Auxiliary Measurements

Continuous EC measurements for water vapor, CO_2, CH_4, and sensible heat fluxes have been conducted at a long-term flux setup installed on the Rush Ranch main tower at 3.4-m height, investigating the influence of tidal inundation on the greenhouse gas budget of the marsh (Knox et al., 2018). In addition, environmental sensors measuring soil temperature, water level, incoming and reflected photosynthetic active radiation (PAR), ground heat flux (G), and net radiation (R_{net}) were operated at an ancillary station, approximately 100 m west from the main tower (Figure 1), within the marsh ecosystem and the main tower flux footprint. Salinity was measured at a long-term water quality monitoring station *SFBFMWQ* (NERRS: NOAA National Estuarine Research Reserve System, 2016), approximately 800 m southwest from the flux tower.

2.3. Flux Errors and Quality Control

By propagating instrumental noise in GC-MS and GC-ECD analysis into the REA flux calculation (equation (1)), we investigated random flux errors (E_{REA}). Analytical precision (σ_c) was calculated as one standard deviation of repeated (n = 3) analysis runs of each sample flask and multiplied by 2 (to account for upsample and downsample):

$$E_{REA} = b\ \sigma w\ 2\sigma_c \tag{5}$$

The distribution of random flux errors is shown in (Figure S5). Accordingly, median relative uncertainties were 7% for CH_3Cl and 18% for CH_3Br.

For chamber fluxes, 90% confidence bounds of the linear fit (dx/dt) for each incubation were used to calculate a high and a low slope/flux. The error estimate (E_{FC}) was defined as the absolute difference between high and low flux

$$E_{FC} = |F_{FC(high)} - F_{FC(low)}| \tag{6}$$

Throughout this manuscript individual hourly fluxes are presented and plotted ± respective flux error estimate. Average fluxes, on the other hand, are reported ± standard deviation within the temporal averaging domain.

The quality of REA fluxes was evaluated by applying the nonstationarity test (Foken & Wichura, 1996) on high-frequency covariances of vertical wind speed and sonic temperature. Only 9 half hour intervals were found to be outside of best quality in regard to stationarity (<30% deviation between ensemble and 5-min covariances). Of these, two REA periods indicated apparent uptake. However, none of these 30-min periods yielded poor results (>100%, where Foken & Wichura, 1996, suggest exclusion of data) and showed no other irregularities (e.g., extremely large variances in high-frequency data of w or T, leading to a questionable b factor, nor extremely high values of σw). Assessment of modeled (Foken & Wichura, 1996) and measurement based integral turbulence characteristics ($\frac{\sigma_w}{u*}$) of the nine identified half hours revealed that turbulence was well established. In a conservative quality control (QC) routine, fluxes were only discarded from further analysis when wind direction measurements indicated source inhomogeneity (wind coming from an adjacent pasture) and possible flow distortion by the tower structure (n = 3).

2.4. Gap Filling Flux Time Series

2.4.1. Daily Scale

Most of the measurements occurred during daylight hours; thus, the calculation of daily fluxes needs to account for diurnally in emissions. To correct for noncontinuous and incomplete sampling for each field outing, two approaches were used. In approach *COSINE*, time series were gap filled, assuming that the diel pattern of methyl halide emissions can be adequately described by a cosine function, the structure of

which was fitted to data from the diurnal case study day (Text S3/S4). In approach *RESPONSE*, 30-min gaps for each field outing were gap filled with parameterized fluxes based on observed temperature response curves. These gap-filled data sets were summed up for each sampling day. The resulting daily emissions were on average 58 ± 8% smaller than diurnal fluxes calculated by simply extrapolating the averaged daytime measurements, demonstrating the importance of gap filling for upscaling purposes.

Temperature response functions were calculated for two data sets: (a) 30-min REA measurements (n = 85) and (b) a merged data set (n = 113) of 30-min REA fluxes and FCs of *L. latifolium* only (n = 28) to obtain a data set spanning over an extended (10–50 °C) temperature range (chamber air temperature was 1.1 to 1.4 times higher than ambient air temperatures, despite the use of outer reflective insulation). It is well documented that plants can produce methyl halides enzymatically. Certain methyltransferases can catalyze the methylation of chloride, bromide, and other halogens, using the methyl donor S-adenosyl-L-methionine (Attieh et al., 1995; Manley, 2002; Rhew et al., 2003; Saini et al., 1995; Wuosmaa & Hager, 1990). Activity rates of enzyme-catalyzed reactions increase with temperature toward an optimum. Higher temperatures cause denaturation or inactivation of enzymes (thermal stability), leading to a steep decline in enzymatic activity (Peterson et al., 2007). Absolute value for optimum temperatures was found to vary between species, development phase, and time but is usually >30 °C (Thapar et al., 2001; Villa et al., 2006). This relationship can be parameterized following the thermodynamic modeling approach of (Sharpe & DeMichele, 1977). Methyl halide emissions as a function of the temperature response of enzymatic activity *F (T)* were fitted to bin medians using nonlinear least squares optimization:

$$F(T) = \frac{E_{\mathrm{opt}} C_{T2} e^{C_{T1} x}}{C_{T2} - C_{T1}\,(1 - e^{C_{T2} x})} \text{ with } x = \frac{T_{\mathrm{opt}}^{-1} - T^{-1}}{R}, \tag{7}$$

where C_{T1} and C_{T2} are empirical coefficients, $E_{\mathrm{opt}}$is the maximum emission capacity at temperature T_{opt}, T is the measured temperature in (K), and R is the universal gas constant (0.00831 kJ · mol^{-1} · K^{-1}). The parameterization follows a unimodal function peaking at $T_{\mathrm{opt}}$and describes lower emission toward both ends of the temperature spectrum. Equation (7) has been used in this or similar formulations in the past to describe isoprene and monoterpene (Guenther et al., 1993) and MBO (Harley et al., 1998) emissions and is currently used as one of two temperature modules in the widely used Model of Emissions of Gases and Aerosols from Nature (MEGAN2.1, Guenther et al., 2012).

Additionally, a much simpler response model (the second temperature module in MEGAN2.1) was used:

$$F(T) = F_{\mathrm{ref}}\, e^{(\beta(T - T_{\mathrm{ref}}))}, \tag{8}$$

where β is an empirical coefficient, and $F_{\mathrm{ref}}$is the flux at temperature T_{ref} = 303 K. Normalizing equation (8) by F_{ref} allows comparing temperature responses of different compounds. In contrast to equation (7), emissions calculated by equation (8) increase steadily with temperature (Figure 4).

2.4.2. Annual Scale

Using both the cosine-derived daily sums and the temperature gap-filled daily sums, full-year continuous time series were then generated with daily resolution using two additional methods to gap fill days in between field outings. In method (FOURIER), a Fourier function was fitted to n = 15 measured daily emissions (Text S4). In method (STEP), a more discrete *step function* approach was used, by assuming constant emissions for each month of measurements (Text S5). Thus, four types of gap filling were employed through the combination of gap-filling approaches within and between days (COSINE-FOURIERF, COSINE-STEP, RESP-FOURIER, and RESP-STEP).

2.5. Diurnal Case Study Day

On 23 August 2016, a warm and sunny day with temperatures ranging from 14 to 25.4 °C, REA measurements (n = 11) were taken between 5:30 and 22:30 PST with the goal of capturing the flux variability of the full day. During sampling the wind direction was stable WSW with minimal variation, resulting in a typical marsh flux footprint. Turbulence was well established between 04:00 and 20:00 PST (Figure 2). During night, negative sensible heat fluxes indicated a stable nocturnal boundary layer ($z_m - z_d/L$ = 0–0.4). Hence, one REA measurement at 22:30 PST was possibly impaired by thermal stratification but did not violate QC tests (section 2.3).

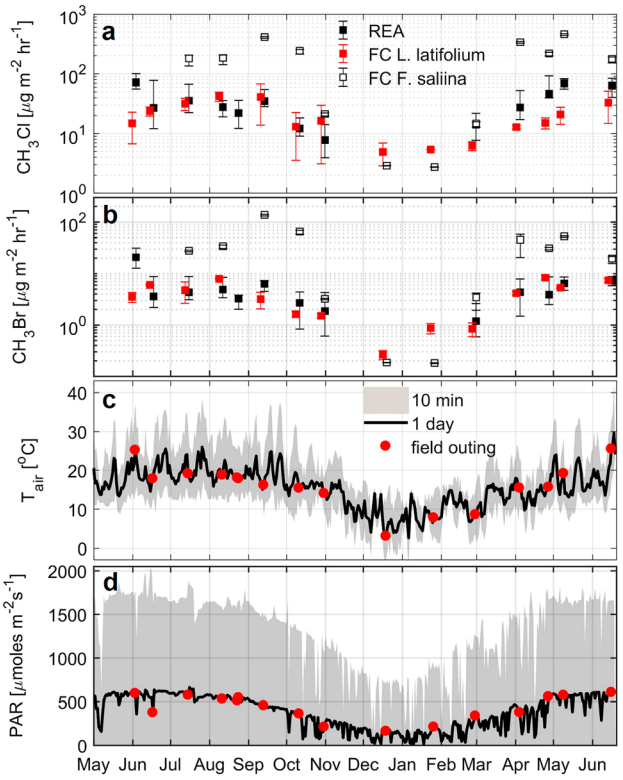

Figure 2. (a) Methyl chloride and (b) methyl bromide fluxes measured by relaxed eddy accumulation (REA) and flux chambers (FC); (c) temperature; and (d) photosynthetic active radiation (PAR) at Rush Ranch tidal marsh from May 2016 to June 2017. Measured daytime (10–16 PST) flux medians (black squares) and ranges (black error bars). *Lepidium latifolium* flux chambers (red squares and error bars for mean ± sd, $n = 2$) and *Frankenia salina* flux chambers (hollow squares) with flux uncertainty from equation (5) (error bars). Lower two panels show daily variation (gray patch), daily averages (black line), and average conditions during gas flux sampling (red dot).

2.6. Upscaling to Global Context

2.6.1. Global Tidal Marsh Area

To keep our upscaling estimates consistent with previous studies, we use the total global tidal marsh area of 0.38×10^{12} m^2 (Woodwell et al., 1973). In light of the reported loss of tidal wetlands across the globe in the order of 1% to 2% per year (equaling ≈ 3,800 to 7,600 km^2/year; Duarte et al., 2005; Crooks et al., 2011; Pendleton et al., 2012), the global salt marsh inventory from Woodwell et al. (1973) is likely outdated. Applying the loss rates iteratively over a period of 44 years yields an updated tidal marsh area of 1.6 to $2.5 \cdot 10^{11}$ m^2, a substantial reduction of 34% to 57%. Integrating the total area of salt marshes mapped by Mcowen et al. (2017), who used a variety of data sources including United Nations Environment Program - World Conservation Monitoring Centre (UNEP-WCMC), (non)governmental and local databases, as well as peer reviewed publications and gray literature, yields a total area of $0.5 \cdot 10^{11}$ m^2, an even lower estimate than our update of the Woodwell et al. (1973) number. Note that Mcowen et al. (2017) claim that their inventory is missing notable marshes in Canada, Northern Russia, South America, and Africa and is thus likely biased low. Further, it remains uncertain if and how global area estimates differentiated between salt and brackish tidal marshes. If area estimates are only representative for the downstream (salt) marshes, the total global tidal wetland area might be larger than suggested here. To account for varying estimates of global tidal marsh area, we calculate a range global of fluxes using the McOwen number as a low end and the update of the Woodwell inventory as a high end 0.5 to $2.5 \cdot 10^{11}$ m^2.

2.6.2. Weighting for Climate Zone and Presence of Halophyte Genus Batis

We classified globally identified and mapped salt marshes (Mcowen et al., 2017) into climate zones (using Köppen-Geiger system, observed data: 1951–2000; Rubel & Kottek, 2010). For the temperate climate zone without a dry season (Cf), which contains the Gulf and East Coast of North America and large parts of coastal Europe, we divided salt marshes into two subgroups based on the presence or absence of the *Batis* genus United States Department of Agriculture - Agricultural Research Service (USDA-ARS, 2015), which has been demonstrated to be an extraordinarily large emitting species (Manley et al., 2006; Rhew et al., 2000, 2014). A weighted emission average was calculated by multiplying each group's relative spatial contribution with the most representative emissions report from the literature ($F_{ref,}$ Table S4a).

3. Results

3.1. CH_3Cl and CH_3Br REA Fluxes: Seasonal Scale

The studied marsh is a continuous source for CH_3Cl and CH_3Br throughout the year, with maximum fluxes during warmer months in the growing season and small but positive fluxes during nongrowing season in winter.

Ecosystem methyl halide fluxes show large variability with time. Average daytime emissions were highest in June (71.8 and 20.5 $\mu g \cdot m^{-2} \cdot hr^{-1}$ for CH_3Cl and CH_3Br, respectively) and lowest in the winter months November till March (7.8 and 1.1 $\mu g \cdot m^{-2} \cdot hr^{-1}$ for CH_3Cl and CH_3Br, respectively; Figure 2). Two monthly measurements show deviations from this seasonal trend: The November measurements are notably high, despite comparably low ambient temperatures. During measurements on 4 June highest REA fluxes for both methyl halides were recorded, coinciding with record high temperatures (Figure 2).

3.2. FCs and Species Specific Production Rates

FC measurements taken during December and February (when no REA measurements were taken because the prevailing winds were from the east) confirm the trend of lowest emissions during the coldest months of the year, with minimum fluxes of 5.7 and 0.2 $\mu g \cdot m^{-2} \cdot hr^{-1}$ (CH_3Cl and CH_3Br, respectively) for

Table 1
Annually Averaged Methyl Halide Production Rates for Different Marsh Vegetation Species

	Halophyte species					
Production rate (year)	*Lepidium latifolium*[a]	*Frankenia salina*[a]	*Frankenia grandifolia*[b]	Batis[b]	Salicornia ssp. ssp. [c]/[b]	*Spartina foliosa*[b]
μg CH_3Cl/gfwt	233	2,294	1,900	420	2.2	18
μg CH_3Cl/gdwt	391	5,805	5,100	2,600	1.4/16	70
μg CH_3Br/gfwt	36	398	260	67	0.6	4
μg CH_3Br/gdwt	71	893	700	420	0.8/4.3	16
μg CH_3I/gfwt	42	15	23	5.5	0.38	11
μg CH_3I/gdwt	120	46	62	34	2.7	44

[a]This study. [b]Manley et al. (2006). [c]Rhew and Mazéas (2010).

L. latifolium and of 2.9 and 0.16 $\mu g \cdot m^{-2} \cdot hr^{-1}$ (CH_3Cl and CH_3Br, respectively) for *F. salina* (Figure 2). Chamber incubations during the warm period of the year reveal large variability in methyl halide emissions between the two studied plant species. Emissions from *F. salina* plots between April and October are a factor of 15 ± 8 and 17 ± 16 (CH_3Cl and CH_3Br) higher than those from *L. latifolium* plots. Winter emissions from *F. salina* plots are lower than the ones observed for *L. latifolium* plots. Averaged over the full annual cycle, *F. salina* emissions are by factors of 10 and 11 higher than emissions from *L. latifolium* plots.

Paired measurements from *L. latifolium* chambers agreed on average within 11% and 45% (CH_3Cl and CH_3Br) but showed occasional large discrepancies (up to factors of 2 and 5) that coincided with shifts in biomass (CH_3Cl), for example, during the onset of senescence. Redeker et al. (2002) conducted experiments on intra-field variability in methyl halide emissions from a rice paddy and found that increasing paired chambers from 2 to 4 yielded an improvement in measuring the *real* (i.e., the mean of all chambers) flux, but probabilities of measuring within 20% of the ensemble mean were still low and varied by season. Despite the close proximity of our FC plots (a few meters), we observed a time lag (1 to 2 weeks) in major biomass dieback between the two *L. latifolium* stands. Largest discrepancies in paired CH_3Br flux measurements occurred during low emission periods in winter. Thus, FC measurements in dynamic natural ecosystems have limitations in precisely quantifying ecosystem-scale fluxes, a shortcoming we address by evaluating the REA method.

Biomass-normalized emissions reveal large interspecies variation in methyl halide emissions: *F. salina* is a very high emitting marsh plant, releasing on average 10 to15 times more CH_3Cl and 11 to 13 times more CH_3Br than *L. latifolium*. *L. latifolium*, however, was found to be the more dominant CH_3I emitter. Production rates for *F. salina* from this study (2,300 μg CH_3Cl and 398 $\mu g\ CH_3Br \cdot gfwt^{-1} \cdot year^{-1}$) agree well with reports from Manley et al. (2006) measured in Southern California (Table 1). If we assume that *S. pacifica* at Rush Ranch has similar emissions as *S. spp*. in Southern California, *L. latifolium* would still emit 25 to 106 (CH_3Cl), 17 to 60 (CH_3Br), and 44 to 111 times more CH_3I than *S. ssp*. These ratios increase by a factor of 11 (CH_3Cl) and 5 (CH_3Br) in respect to *S. spp*. reference fluxes from China Camp (Northern California). Despite the high spatial coverage of *S. pacifica* at Rush Ranch (in three analyzed vegetation transects, *S. pacifica* coverage is 2.8 times *L. latifolium* coverage) this species may only be of minor importance for the marsh's methyl halide budget.

Biomass halide content (see section 2.2.4) varied between the halophyte species, with highest contents in *F. salina* tissue, ranging from 3.7 to 104 g Cl^-/kg and 0.2 to 3.1 g Br^-/kg, respectively. *L. lepidium* tissue samples ranged between 0.2 to 50 g Cl^-/kg and 0.06 to 2.4 g Br^-/kg. The highest halide contents of both species were observed in the September samples, that is, during onset of senescence, whereas lowest halide contents were found in dead plant tissue during winter sampling. In addition to halide concentration variability associated with plant growth stage, there was also interannual variability in the soil water salinity which likely influenced the tissue halide content, with an enrichment in the drought year 2016 as compared to the wet year of 2017 (Figure S3). Absolute values of *L. latifolium* samples were similar to those from Sherman Island, California (Khan et al., 2013), with maxima of 51 g Cl^-/kg and 1.1 g Br^-/kg during senescence. *F. salina* content in this study was roughly half of reports from the coastal Upper Newport Bay saltmarsh of 200 g Cl^-/kg and 2.8 g Br^-/kg (Manley et al., 2006), reflecting the salinity gradient between the brackish marsh (this study) and the salt marshes in Southern California.

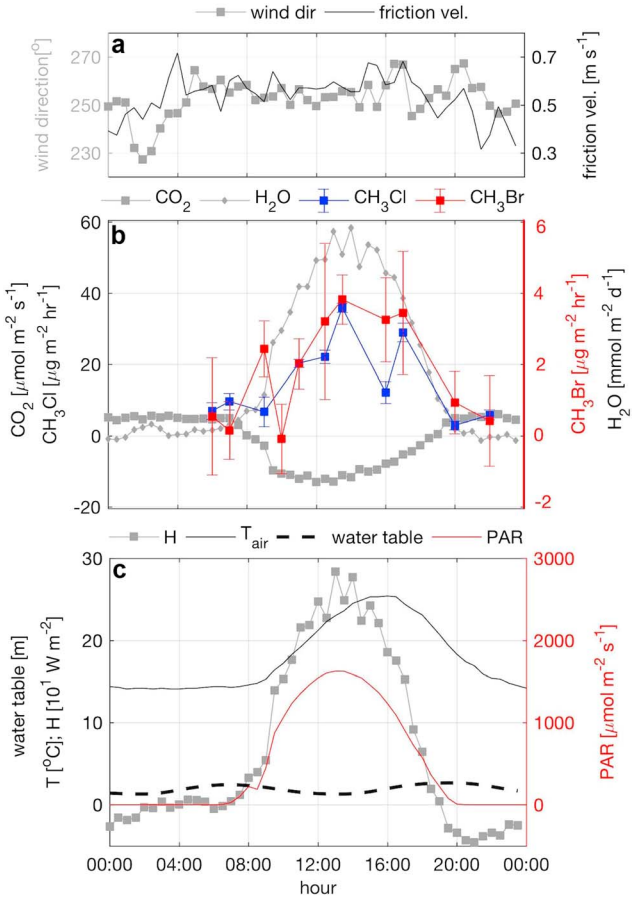

Figure 3. Diurnal measurements on 23 August 2016. Panel a: Time series of wind direction and friction velocity. Panel b: Flux measurements of CO_2 (gray squares) H_2O (gray diamonds), CH_3Cl (blue squares), CH_3Br (red squares). Panel c: Ambient temperature (black line), sensible heat fluxes H (squares), water table depth (black dashed line), and photosynthetic active radiation (PAR; red line).

3.3. CH_3Cl and CH_3Br Fluxes: Diel Scale

CH_3Cl and CH_3Br emissions follow a diel pattern (Figure 3), with minimum fluxes during the night and early morning and maximum fluxes between 13 to 17 PT. Daytime emissions are factors of 4.5 (CH_3Cl) and 7 (CH_3Br) higher than nighttime fluxes. Nighttime measurements of CH_3Cl indicate emissions, whereas flux errors of apparent CH_3Br emissions cross the zero line and; hence, we cannot completely rule out that observed nighttime emissions are not different from zero. During the case study day, diel flux patterns of methyl halides were significantly correlated to (in order of Spearman rank correlation coefficient) diurnal variations in ecosystem evapotranspiration (R = 0.83), PAR, and CO_2 flux (R = 0.76), and ambient temperature (R = 0.68). The better correlation to evapotranspiration as compared to radiation or sensible heat stems from longer lasting daytime peak emissions. As a result, methyl halide emissions decline in synchronicity with temperature drops in the afternoon.

3.4. Light and Temperature Response of Ecosystem Fluxes

Half-hourly methyl halide fluxes showed correlations to temperature with rank-sum coefficients of r_s = 0.67 CH_3Cl and r_s = 0.44 CH_3Br, respectively. Nonlinear response functions (equations (7) and (8)) were found to describe observed flux patterns better than linear ones. Comparing the two different temperature response parameterizations showed that the first-order exponential response (equation (8)**)** yielded smaller residuals (RMSE = 4.5 $\mu g \cdot m^{-2} \cdot hr^{-1}$) and a larger coefficient of determination compared to equation (7) (Table 2**)**. We conditionally sampled the 30-min fluxes by temperature into groups of 4 °C temperature increments, to account for an unequal distribution of observed fluxes across the temperature range. Response functions were fitted on averaged fluxes within each temperature bin.

Correlations of 30-min emission data with incident light (Figure S3) are less pronounced and show more scatter than the ones to temperature. Rank-sum coefficients were R = 0.60 (CH_3Cl) and R = 0.40 CH_3Br (more results in Text S6 and Table S3). To test the effect of lagged relationships, cross-correlation analysis was performed. However, correlation was not improved by lagging time series of PAR up to 1 day.

3.5. Soil Core Fluxes

Soil core incubation results indicate that the brackish marsh soil at Rush Ranch is, at the time of soil sampling in spring, both a small source for CH_3I and a small source and sink for CH_3Cl and CH_3Br (Table 2). Observed soil source was by a factor of 300 (CH_3I), 80 (CH_3Cl) to 70 (CH_3Br) smaller than studied vegetation sources. Soil

Table 2
Fitting Results for Temperature Response Functions (Equations (7) and (8)), and Fit Evaluation Based on Bin-Averaged Flux Medians, Grouped Into 4° Temperature Classes

	Coefficient					
Compound	C_{T1}	C_{T2}	E_{opt} ($\mu g \cdot m^{-2} \cdot hr^{-1}$)	T_{opt} (K)	r^2	RMSE
CH_3Cl	80.3 [46 115]	199 [129, 269]	55.8 [45, 66]	307	0.89	6
CH_3Br	106.9 [72, 141]	188.2 [152, 225]	9.4 [8, 11]	307	0.92	0.65
	F_{ref} ($\mu g \cdot m^{-2} \cdot hr^{-1}$)	β			r^2	RMSE
CH_3Cl	54.1 [45, 63]	0.083 [0.05, 0.12]			0.97	4.5
CH_3Br	8.2 [7, 9]	0.099 [0.08, 0.12]			0.99	1

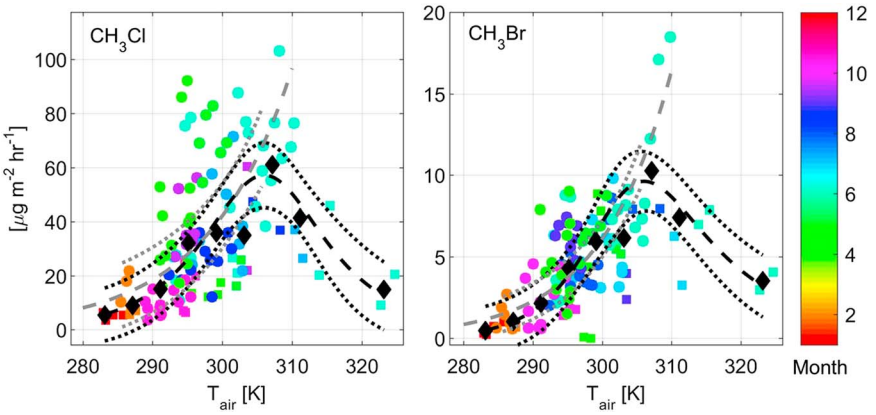

Figure 4. Temperature response of methyl halide emissions, measured by Relaxed Eddy Accumulation (circles) and *Lepidium latifolium* flux chambers (squares), color coded by month of measurement (color map). Overlaid are bin medians (black diamonds) and two fitted functions: Equation (7) (black dashed line) with 90% prediction bounds (black dotted line) and equation (8) (gray dashed lines).

uptake is in the order of 1.2 (CH_3Cl) and 0.2 (CH_3Br) % of observed net emissions from vegetation. Regarding CH_3I, sampled soil cores were exclusively sources, with highest emissions from the wettest soil core incubated.

4. Discussion

4.1. Light and Temperature Responses

Diel patterns in methyl halide emissions have been observed across all studied marshes, suggesting strong influences of either light and/or temperature. For example, in a partial and complete shading experiment (Blei et al., 2010) and during paired incubations in both transparent and opaque chambers (Rhew & Mazéas, 2010), no significant differences in emissions under different light conditions were observed. In contrast, stronger correlations between emissions and PAR versus temperature were found in Irish and Scottish coastal wetlands (Dimmer et al., 2001; Drewer et al., 2006). It is questionable how well PAR and temperature can be differentiated in a simple single explanatory variable regression analysis, since temperature and light can be strongly intercorrelated, and methyl halide flux time series were too infrequent in time (usually $<$10 measurements per day) to capture response times well.

For extended periods of this study, REA fluxes agree well with emissions based on incubation measurements of *L. latifolium* in opaque chambers. Arguably, this is not as direct of a controlled experiment as performed by Blei et al. (2010) and Rhew and Mazéas (2010), but it serves as an indication for non-light-dependent methyl halide emissions from halophytes, at least for immediate emissions in time scales of minutes to a few hours. This hypothesis is supported by positive fluxes during night, observed during the diurnal case study day (Figure 3) and was confirmed by cross-correlation analysis of REA fluxes and lagged PAR observations, yielding the highest correlation at 0 lag.

Results from fitted temperature response curves (Figure 4) of merged REA and FC data set support a nonlinear and unimodal response to ambient temperature, peaking at 307 K (34 °C), which can be adequately described by equation (7). Temperature-limited emissions can well be illustrated by comparing the REA and *L. latifolium* FC measurements. For most outings, the REA and *L. latifolium* FC measurements fall in the same temperature bin and yield similar magnitude of fluxes. However, on the measurement day in June 2016, a striking disagreement occurred between the REA and *L. latifolium* chamber measurements. Sampling occurred during a 10-day-lasting heatwave with clear-sky and ambient temperatures up to 311 K (38 °C). Due to imperfect temperature control of the enclosures, chamber air warmed up to $>$320 K (50 °C) during incubation. As may be expected for enzymatic reactions, these extreme temperatures resulted in substantially lower fluxes.

Through the use of the temperature modules from MEGAN, fitted parameters can be compared to other volatile organic compounds. Accordingly CH_3Cl and CH_3Br responses (slope $\beta = 0.08$ and $\beta = 0.10$) lie in between

reports for ethanol (β = 0.07) on the lower end and monoterpenes and the biogenic stress VOC ethene (β = 0.11) on the higher end (Kaser et al., 2013; Rhew et al., 2017).

If plotted as a function of light, methyl halide emissions show a seemingly exponential increase (Figure S3 and Text S6). The observed relationship is different from commonly used photosynthesis models, which generally follow a parabolic Michaelis-Menten equation, meaning that photosynthetic rate asymptotes at high light availability (Lin et al., 2015). Low correlation coefficients stem from large variability in halide emissions at high light levels (PAR $\geq$ 1,500 $\mu mol \cdot m^{-2} \cdot s^{-1}$). Emissions under these light conditions vary by a factor of 5 (Figure S3). This light intensity was reached from April to September (Figure 2). Especially during the marsh vegetation maturation phase in late summer, methyl halide emissions decreased (dark blue circles, Figure S3), whereas peak emissions (up to 5 times higher) were measured during the onset of flowering (light green, Figure S3) and during the hottest day of the year in early summer (cyan, Figure S3). We conclude that during the growing and especially during the flowering season, when highest emissions were observed, methyl halide fluxes can only poorly be constrained by light alone. We hypothesize that light availability may have effects on the marsh vegetation metabolism and availability of halide precursors but is not the controlling factor for methyl halide emissions on shorter time scales (e.g., hours to 1 day).

4.2. Water Table, Flooding, Soil Water Content, and Salinity

Methyl halide fluxes show only a weak correlation (R = 0.26) with soil water salinity measurements conducted at the ancillary tower (Figure 1). This is probably a local effect tied to interannual variability in hydrological patterns (Figure S4): highest salinity (9‰) was reached at the end of the dry season (mid-October, 2016, a drought year in California), steadily decreased to minimum values around 1‰ throughout the rainy winter of 2016/2017, and remained low for the growing season of 2017. This pattern is desynchronized with seasonal patterns of halide emissions. No significant difference between emissions in the flowering season of the dry year 2016 and the wet year of 2017 were found. However, CH_3Cl fluxes of senescent halophytes in September 2016 were notably high, coinciding with high salinity and maximum tissue halide content, indicating a potential relationship between methyl halide emissions and salinity. However, our measurements cannot fully constrain this relationship due to noncontinuous sampling and large interannual variability.

Similarly, only weak correlations with water table fluctuations (R = 0.06) or inundated periods were found. Water table fluctuations were mainly driven by semidiurnal tides, and at longer time scales, by alternating spring and neap tides, with water levels at or above local sediment surface during spring tides and below surface during neap tides.

Marsh plain flooding occurred only during new moon spring tides in summer and full moon spring tides in winter (approximately every 29 days). Whereas flooding was found to significantly reduce ecosystem respiration (CO_2 emissions) at Rush Ranch, no direct effect on gross primary production (CO_2 uptake) was found (Knox et al., 2018). Similarly, also for methyl halide fluxes, no correlation with water table fluctuations was found. It remains to be answered if correlations on shorter time scales would have been revealed by continuous flux measurements. Especially during night, when ecosystem respiration drives net ecosystem exchange, almost no methyl halide measurements were conducted and hence the effect of flooding might be masked by sampling frequency. Flooding which occurred near midnight in summer when diel patterns of methyl halide fluxes showed near zero emissions, and near noon in winter (the season with lowest halide emissions) might reduce emission from abiotic methyl halide sources, such as leaf litter decomposition from the topsoil layer (Hamilton et al., 2003) due to enhanced diffuse resistance in the water layer and a cooler microclimate. High SWC, on the other hand, was found to increase emissions from bare soil. However, on an annual time scale, these fluxes were negligible (section 3.5). It should be noted that prolonged periods of flooding, for example, induced by management actions, are known to potentially cause directional changes in marsh vegetation composition, distribution, and biomass (Tobias et al., 2016) and could potentially weaken *L. latifolium's* source strength at Rush Ranch if flooding frequency and duration increase in the future.

4.3. Soil Versus Vegetation Source

At the Rush Ranch marsh, methyl halide emissions were predominantly associated with the standing halophytic vegetation. This is evident when comparing the large emissions from the vegetated FCs compared

Table 3
Methyl Halide Fluxes From Soil Core Incubations as Functions of Volumetric Soil Water Content Measured During Soil Core Collection

Soil Water Content (%)	Flux	CH_3Br	CH_3Cl	CH_3I
40	$ng \cdot m^{-2} \cdot hr^{-1}$	−9.5	−450	1.8
	std	8	156	2.6
50	$ng \cdot m^{-2} \cdot hr^{-1}$	−8.3	−245	6.7
	std	7.1	90	3.1
60	$ng \cdot m^{-2} \cdot hr^{-1}$	55	258	29.5
	std	36	137	5.6

Note. Standard deviations result from replicated samples (n = 2) and repeated incubations (n = 2) of each soil water content class.

to the negligible fluxes from the bare soil cores. This finding is in line with studies conducted in Southern California salt marshes (Rhew et al., 2000, 2002; Manley et al., 2006).

Our soil core incubation results (Table 3) indicate a trend of increasing methyl halide production with soil water content: wet soils (SWC ≈ 60%) of the lower marsh were found to be an exclusive source, whereas fluxes from soil cores from higher parts of the marsh yielded net consumption. Highest uptake was measured in the driest soil cores analyzed (SWC 40%). This finding is in line with reports from Khan et al. (2012), who used stable isotope tracers to measure gross consumption and production fluxes of methyl halides from peatland soils at Sherman Island (≈ 30 km south east of Rush Ranch) and describe a parabolic relationship between SWC and gross consumption, peaking at 30% SWC. Toward both drier and wetter soils, consumption declines. At 60% SWC, consumption is almost entirely suppressed, which could explain the exclusively positive fluxes we measured at Rush Ranch from the wet soils sampled in the lower marsh, and the highest net uptake measured at the 40% SWC cores. Absolute values between both studies agree fairly well, with Rush Ranch to Sherman Island net flux ratios of 1.9 (CH_3Cl) and 1.1 (CH_3Br) at comparable SWC levels.

4.4. Implication of Heat Waves

Largest emissions at Rush Ranch were measured during a 7-day heat wave (five consecutive days with daily maximum temperatures >30 year average of maximum temperature) in June 2016. Integrated fluxes yield emissions of 940 μg CH_3Cl and 280 μg CH_3Br per day. These emissions deviate from a modeled harmonic seasonal fluctuation, by 20% (CH_3Cl) and up to 100% (CH_3Br). This finding indicates that frequency and duration of heatwaves might have a significant effect on total annual emissions and that these emissions are partly desynchronized from seasonal fluctuations of ambient temperature and the plant growing cycle. Historically, heatwaves occur on average 6.5 times per year between days of year 120 to 280. Accordingly, the years of our field study were of high heat stress with 8 and 12 heatwaves in 2016 and 2017, respectively. Due to noncontinuous sampling, we are unable to precisely resolve the importance of heatwaves on ecosystem emissions. Nevertheless, a simplified example can be used: during time of sampling, n = 65 unique heatwave days were identified. If we raise the daily emissions from identified days in our Fourier-interpolated data set by 20% for CH_3Cl and 100% for CH_3Br, the annually integrated emissions increase by 24% to 273 μmoles $CH_3Br \cdot m^{-2} \cdot year^{-1}$ and by 7% to 2,852 μmoles $CH_3Cl \cdot m^{-2} \cdot year^{-1}$.

4.5. Assessing Biological Invasion by *L. latifolium*

Our results demonstrate substantial methyl chloride and methyl bromide emissions from pepperweed (*L. latifolium*). Pepperweed is the third strongest emitting wetland species (outside of the tropics) identified thus far, being very close to number 2 (*Batis maritima*; Table 1). However, our results indicate that *L. latifolium* is the largest emitter of CH_3I. In contrast to *L. latifolium*, the *B. maritima* geographical distribution is less widespread and mostly limited to Atlantic and Pacific tropical coasts (USDA-ARS, 2015). Today, *L. latifolium* occurs in the entire latitudinal range of California, populating coastal and interior wetlands. It tolerates fresh, brackish, and to certain extent saltwater systems and can also be found around agricultural fields. Combining the observed emissions, the extraordinary high invasion potential and the expansion trend of *L. latifolium*, we hypothesize that ongoing pepperweed invasion is likely to increase methyl halide emissions from brackish wetlands. *L. latifolium* may also increase emissions from tidal marshes with *F. salina* or *B. maritima*, if it does not exclude these two natives but rather outcompetes other nonhalide emitting species, as has been observed in the past (Boyer & Burdick, 2010; Tobias et al., 2016). At Rush Ranch, the microhabitats of *F. salina* and *L. latifolium* were clearly separated, with *F. salina* populating the drier parts of the marsh, allowing cooccurrence of both methyl halide emitting species.

4.6. Annual CH_3Cl and CH_3Br Fluxes

Four different approaches were used to compute interpolated annual time series, based on diurnally averaged fluxes (n = 15 measurement days), which were either gap filled based on a cosine model or temperature response curve.

Table 4
Annual Emission Estimates for Four Different Gap-Filling Approaches

Compound		Method	$\mu moles \cdot m^{-2} \cdot year^{-1}$	$mg \cdot m^{-2} \cdot year^{-1}$
CH_3Cl	COSINE-FOURIER		3,040	154
	COSINE-STEP		2,438	123
	RESPONSE-FOURIER		2,589	131
	RESPONSE-STEP		2,594	131
		Ensemble Average	2,665	135
		sd	260	13
CH_3Br	COSINE-FOURIER		197	19
	COSINE-STEP		193	18
	RESPONSE-FOURIER		257	24
	RESPONSE-STEP		2,356	22
		Ensemble Average	221	21
		sd	31	3

The resulting estimates for annual emissions (Table 4) from the studied marsh agree well between the four different approaches with ensemble averages (± sd) of 135 ± 13 and 21 ± 3 $\mu moles \cdot m^{-2} \cdot year^{-1}$ (CH_3Cl and CH_3Br). A simple error propagation of random flux errors of half hourly flux observations and the observed gap-fill uncertainty, that is, the range between the four different approaches, yielded relative uncertainties of 22% for CH_3Cl and 33% for CH_3Br with respect to the annual fluxes reported in (Table 4). These annual emission estimates are remarkably close to reports from salt marshes in Southern California: 132 mg $CH_3Cl \cdot m^{-2} \cdot year^{-1}$ and 21 mg $CH_3Br \cdot m^{-2} \cdot year^{-1}$ (Manley et al., 2006), where 3 years of biweekly FC incubations were carried out over different vegetation stands, mud flats, and barren soil, to obtain an ecosystem scale flux, similar to this study.

4.7. Upscaling to a Global Context

Coastal salt marshes are believed to be globally significant sources of both CH_3Cl and CH_3Br. In the most recent WMO/UNEP Assessment of Ozone Depletion (Carpenter et al., 2014), salt marsh emissions are estimated at 85 (which is the midpoint of all reported extrapolations which ranged from 1.1 to 170) and 7 (0.6 to 14) Gg/year for CH_3Cl and CH_3Br, respectively. The lowest saltmarsh extrapolations (1.1 Gg CH_3Cl and 0.6 Gg CH_3Br/year) are based on a (cool) temperate climate coastal wetland in Tasmania (41°S; Cox et al., 2004). Similarly, low extrapolations (2 to 10 Gg CH_3Cl and 0.8 to 1.1 Gg CH_3Br/year) are based on temperate salt marsh sites in Scotland, also at a relatively high latitude (54–56°N; Blei et al., 2010). In contrast, the highest extrapolations (160 to 170 Gg CH_3Cl and 8 to 14 Gg CH_3Br/year) are based on Mediterranean climate salt marshes in Southern California (32°N; Manley et al., 2006; Rhew et al., 2000). A more recent study at a subtropical salt marsh in Texas (27 to 28°N) led to even higher potential extrapolations (170 to 326 Gg CH_3Cl and 23 Gg $CH_3Br/year^1$; Rhew et al., 2014). Halophytes in tropical ecosystems might be of relevance as shown by extraordinary high production rates. Yokouchi et al. (2007) report CH_3Cl production rates of 1.6 to 2.8 $\mu g \cdot (g\ dry\ wt)^{-1} \cdot hr^{-1}$ (24°N), which is a factor of 2 to 5 higher than average production rates measured in this study (Table 1).

Based on this literature comparison, it seems reasonable to hypothesize that salt marsh emissions vary by latitude and are strongly influenced by climate, with lowest emissions in cool temperate regions (at higher latitudes) and highest emissions from warm temperate and subtropical zones (at lower latitudes). As described in section 2.7 we evaluated global methyl halide fluxes using climate zone weighted emission inventory, yielding global fluxes of 30.6 CH_3Cl (range: 10.2 to 77.4) and 3.1 CH_3Br (range: 1.0 to 7.8) Gg/year (the ranges account for the low- and high-end estimate of global salt marsh surface area). This exercise indicates that salt marshes are not likely to account for the missing source of the methyl halides. In addition, climate-zone weighted salt marsh emissions are likely to provide a more realistic emission budget than previously published estimates based on single sites or the ensemble midrange estimate from the WMO report. Our upscaling inventory can be modified by future studies (Tables S4a–S4c), especially if more precise tidal marsh area databases become available. Our study suggests that brackish marshes can have comparable source strengths to salt marshes.

5. Conclusions

In this study, a relaxed eddy accumulation sampling system coupled with high-precision gas chromatography allowed for the first ecosystem-scale net flux measurements of methyl bromide and methyl chloride from a coastal brackish marsh, with flux footprints encompassing halophyte vegetation stands, bare soil, and open water. Fluxes show seasonality that generally follows the ambient temperature and growth cycle of the most dominant halophytes, but there are several interesting deviations. First, REA emissions showed markedly high emissions in June and September of 2016 relative to the adjacent months. This suggests that the fluxes are not simply following a seasonal cycle. Second, the REA emissions corresponded more closely to the fluxes of *L. latifolium* plots than *F. salina* plots, even though the latter sites emitted ~10 times more mass per unit area. Third, the emission rates were very large compared to other marshes, even at the higher end of the salinity gradient, at this latitude (Rhew & Mazéas, 2010).

The invasive species *L. latifolium* was found to be a large methyl halide emitter, apparently driving the net ecosystem emissions from Rush Ranch. Our results suggest that the wide spatial coverage of *L. latifolium*, resulting from its high stress tolerance and invasion potential, may more than compensate for its lower methyl halide production rates compared to native species of the genera *Frankenia* and *Batis*. Furthermore, during senescence and over winter, degradation of the thick litter layer associated with *L. latifolium* may have contributed to significant abiotic methyl halide emissions, which were less pronounced for native species with less litter accumulation. As a result, the ongoing biological invasion of *L. latifolium* might increase methyl halide emissions from impacted marsh ecosystems.

Through an upscaling routine, we demonstrate that tidal marshes may contribute up to 1.3% and 5.0% of combined anthropogenic and biogenic emissions (up to 1.6% and 8.6% of biogenic emissions) for CH_3Cl and CH_3Br globally. Hence, tidal marshes are a minor source for stratospheric chlorine, but a notable source for stratospheric bromine globally.

Type of land use change (e.g., drainage for agriculture, natural conversion due to changes in the hydrology, and salinity regime) will ultimately govern future ozone depletion and global warming potential of today's tidal marshes. Our study indicates that emissions from Rush Ranch will increase in a warming climate, especially during periods of heat waves. Seasonal (noncontinuous) sampling can lead to notable biases in interpolated data sets, especially when a disproportionate number of heatwave events are sampled. Temperature response and the extent of biological invasion by *L. latifolium* were found to be the two most important controlling factors of ecosystem-scale emissions of methyl halides from the studied marsh.

Acknowledgments

We recognize outstanding support from Brian Bergamaschi, Lisamarie Windham-Myers, the USGS and San Francisco Bay National Estuarine Research Reserve for establishment and maintenance of the flux tower and monitoring sites, and for data sharing. Further we acknowledge Steve Kohlmann and the Solano Land Trust for facilitating experimental work on their land. Last but not least, we thank numerous helpers from Rush Ranch and the Rhew Lab: Connor Shingai, Charles Li, Anya Mikheicheva, Jerrold Acdan, Bernard Koh, Yujia Tao, Ross Ward, Brendan Smith, and Zach Owens for many hours spent in the field and lab. M. J. Deventer was funded by NSF Atmospheric Chemistry grant 1258365, J. A. Lewis and M. C. Ferner were supported by an award under the Coastal Zone Management Act, administered by NOAA's Office for Coaslal Management, to San Francisco State University. Methyl Halide associated data are available under Creative Commons Attribution (CC-BY) license at UC Berkeley Dash, https://doi.org/10.6078/D1QM2R, and carbon flux data are available under ameriflux policy at doi: 10.17190/AMF/1418685. Meteorological and hydrological data are openly available from the National Estuarine Research Reserve data portal under the San Francisco Bay, CA First Mallard site (http://cdmo. baruch.sc.edu/aqs/).

References

Attieh, J. M., Hanson, A. D., & Saini, H. S. (1995). Purification and characterization of a novel methyltransferase responsible for biosynthesis of halomethanes and methanethiol in Brassica oleracea. *Journal of Biological Chemistry*, *270*, 9250–9257. https://doi.org/10.1074/jbc.270.16.9250

Baker, J. M. (2000). Conditional sampling revisited. *Agricultural and Forest Meteorology*, *104*, 59–65.

Baldocchi, D. D., Hincks, B. B., & Meyers, T. P. (1988). Measuring biosphere-atmosphere exchanges of biologically related gases with micrometeorological methods. *Ecology*, *69*(5), 1331. https://doi.org/10.2307/1941631

Bellue, M. K. (1936). *Lepidium latifolium* L. a new perennial peppergrass. Calif. Dep. Agric. Bull. 25:359.

Blank, R. R., & Young, J. A. (2002). Influence of the exotic invasive crucifer, *Lepidium latifolium*, on soil properties and elemental cycling. *Soil Science*, *167*(12), 821–829. https://doi.org/10.1097/00010694-200212000-00006

Blei, E., Heal, M. R., & Heal, K. V. (2010). Long-term CH_3Br and CH_3Cl flux measurements in temperate salt marshes. *Biogeosciences Discussions*, *7*(4), 6295–6322. https://doi.org/10.5194/bgd-7-6295-2010

Bossard, C. C., Randall, J. A., & Hoshovsky, M. C. (Eds.) (2000). *Invasive plants of California's wildlands*. Berkley, CA: University of California Press.

Boyer, K. E., & Burdick, A. P. (2010). Control of *Lepidium latifolium* (perennial pepperweed) and recovery of native plants in tidal marshes of the San Francisco estuary. *Wetlands Ecology and Management*, *18*(6), 731–743. https://doi.org/10.1007/s11273-010-9193-z

Businger, J. A., & Oncley, S. P. (1990). Flux measurement with conditional sampling. *Journal of Atmospheric and Oceanic Technology*, *7*(2), 349–352. https://doi.org/10.1175/1520-0426

Butler, J. H., King, D. B., Lobert Jürgen, M., Montzka Stephen, A., Yvon-Lewis Shari, A., Hall Bradley, D., et al. (2007). Oceanic distributions and emissions of short-lived halocarbons. *Global Biogeochemical Cycles*, *21*, GB1023. https://doi.org/10.1029/2006GB002732

Callaway, J., Borgnis, E., Turner, R., & Milan, C. (2012). Carbon sequestration and sediment accretion in San Francisco Bay tidal wetlands. *Estuaries and Coasts*, *35*(5), 1163–1181. https://doi.org/10.1007/s12237-012-9508-9

Carpenter, L. J., Reimann, S., Burkholder, J. B., Clerbaux, C., Hall, B. D., Hossaini, R., et al. (2014). Chapter 1: Update on Ozone-Depleting Substances (ODSs) and other gases of Interest to the montreal protocol. In C. A. Ennis (Ed.), *Scientific Assessment of Ozone Depletion: 2014* (Global Ozone Research and Monitoring Project – Report No. 55). Geneva, Switzerland: World Meteorological Organization.

Cox, M. L., Fraser, P. J., Sturrock, G. A., Siems, S. T., & Porter, L. W. (2004). Terrestrial sources and sinks of halomethanes near Cape Grim, Tasmania. *Atmospheric Environment*, *38*(23), 3839–3852. https://doi.org/10.1016/j.atmosenv.2004.03.050

Crooks, S., Herr, D., Tamelander, J., Laffoley, D., & Vandever, J. (2011). Mitigating climate change through restoration and management of coastal wetlands and near-shore marine ecosystems: Challenges and opportunities. Environment department papers; no. 121. Marine ecosystem series. World Bank, Washington, DC. Retrieved from https://openknowledge. worldbank.org/handle/10986/18318, License: CC BY 3.0 IGO.

Dimmer, C. H., Simmonds, P. G., Nickless, G., & Bassford, M. R. (2001). Biogenic fluxes of halomethanes from Irish peatland ecosystems. *Atmospheric Environment*, *35*(2), 321–330. https://doi.org/10.1016/S1352-2310(00)00151-5

Drewer, J., Heal, M. R., Heal, K. V., & Smith, K. A. (2006). Temporal and spatial variation in methyl bromide flux from a salt marsh. *Geophysical Research Letters*, *33*, L16808. https://doi.org/10.1029/2006GL026814

Duarte, C. M., Middelburg, J. J., & Caraco, N. (2005). Major role of marine vegetation on the oceanic carbon cycle. *Biogeosciences*, *2*(1), 1–8. https://doi.org/10.5194/bg-2-1-2005

Foken, T., & Wichura, B. (1996). Tools for quality assessment of surface-based flux measurements. *Agricultural and Forest Meteorology*, *78*(1–2), 83–105. https://doi.org/10.1016/0168-1923(95)02248-1

Gan, J., Yates, S. R., Ohr, H. D., & Sims, J. J. (1998). Production of methyl bromide by terrestrial higher plants. *Geophysical Research Letters*, *25*, 3595–3598. https://doi.org/10.1029/98GL52697

Gebhardt, S., Colomb, A., Hofmann, R., Williams, J., & Lelieveld, J. (2008). Halogenated organic species over the tropical south American rainforest. *Atmospheric Chemistry and Physics*, *8*(12), 3185–3197. https://doi.org/10.5194/acp-8-3185-2008

Guenther, A. B., Jiang, X., Heald, C. L., Sakulyanontvittaya, T., Duhl, T., Emmons, L. K., & Wang, X. (2012). The model of emissions of gases and aerosols from nature version 2.1 (MEGAN2.1): An extended and updated framework for modeling biogenic emissions. *Geoscientific Model Development*, *5*(6), 1471–1492. https://doi.org/10.5194/gmd-5-1471-2012

Guenther, A. B., Zimmerman, P. R., Harley, P. C., Monson, R. K., & Fall, R. (1993). Isoprene and monoterpene emission rate variability: Model evaluations and sensitivity analyses. *Journal of Geophysical Research*, *98*, 12,609–12,617. https://doi.org/10.1029/93JD00527

Hamilton, J. T. G., McRoberts, W. C., Keppler, F., Kalin, R. M., & Harper, D. B. (2003). Chloride methylation by plant pectin: An efficient environmentally significant process. *Science*, *301*(5630), 206–209. https://doi.org/10.1126/science.1085036

Harley, P., Fridd-Stroud, V., Greenberg, J., Guenther, A., & Vasconcellos, P. (1998). Emission of 2-methyl-3-buten-2-ol by pines: A potentially large natural source of reactive carbon to the atmosphere. *Journal of Geophysical Research*, *103*, 25,479–25,486. https://doi.org/10.1029/98JD00820

Hu, L., Yvon-Lewis, S. A., Liu, Y., Salisbury, J. E., & O'Hern, J. E. (2010). Coastal emissions of methyl bromide and methyl chloride along the eastern Gulf of Mexico and the east coast of the United States. *Global Biogeochemical Cycles*, *24*, GB1007. https://doi.org/10.1029/2009GB003514

Jones, C. E., Hornsby, K. E., Sommariva, R., Dunk, R. M., von Glasow, R., McFiggans, G., & Carpenter, L. J. (2010). Quantifying the contribution of marine organic gases to atmospheric iodine. *Geophysical Research Letters*, *37*, L18804. https://doi.org/10.1029/2010GL043990

Kaser, L., Karl, T., Guenther, A., Graus, M., Schnitzhofer, R., Turnipseed, A., et al. (2013). Undisturbed and disturbed above canopy ponderosa pine emissions: PTR-TOF-MS measurements and MEGAN 2.1 model results. *Atmospheric Chemistry and Physics*, *13*(23), 11,935–11,947. https://doi.org/10.5194/acp-13-11935-2013

Khan, M. A. H., Rhew, R. C., Zhou, K., & Whelan, M. E. (2013). Halogen biogeochemistry of invasive perennial pepperweed (*Lepidium latifolium*) in a peatland pasture. *Journal of Geophysical Research: Biogeosciences*, *118*, 239–247. https://doi.org/10.1002/jgrg.20020

Khan, M. A. H., Whelan, M. E., & Rhew, R. C. (2012). Effects of temperature and soil moisture on methyl halide and chloroform fluxes from drained peatland pasture soils. *Journal of Environmental Monitoring*, *14*(1), 241–249. https://doi.org/10.1039/C1EM10639B

Kljun, N., Calanca, P., Rotach, M. W., & Schmid, H. P. (2015). A simple two-dimensional parameterisation for flux footprint prediction (FFP). *Geoscientific Model Development*, *8*(11), 3695–3713. https://doi.org/10.5194/gmd-8-3695-2015

Knox, S. H., Windham-Myers, L., Anderson, F., Sturtevant, C., & Bergamaschi, B. (2018). Direct and indirect effects of tides on ecosystem-scale CO_2 exchange in a brackish tidal marsh in Northern California. *Journal of Geophysical Research: Biogeosciences, 123*. https://doi.org/10.1002/2017JG004048, *123*, 787–806.

Lin, M., Wang, Z., He, L., Xu, K., Cheng, D., & Wang, G. (2015). Plant photosynthesis-irradiance curve responses to pollution show non-competitive inhibited Michaelis Kinetics. *PLoS One*, *10*(11), e0142712. https://doi.org/10.1371/journal.pone.0142712

Manley, S. L. (2002). Phytogenesis of halomethanes: A product of selection or a metabolic accident? *Biogeochemistry*, *60*(2), 163–180. https://doi.org/10.1023/A:1019859922489

Manley, S. L., Wang, N.-Y., Walser, M. L., & Cicerone, R. J. (2006). Coastal salt marshes as global methyl halide sources from determinations of intrinsic production by marsh plants. *Global Biogeochemical Cycles*, *20*, GB3015. https://doi.org/10.1029/2005GB002578

Mcowen, C., Weatherdon, L., Bochove, J.-W., Sullivan, E., Blyth, S., Zockler, C., et al. (2017). A global map of saltmarshes. *Biodiversity Data Journal*, *5*, e11764. https://doi.org/10.3897/BDJ.5.e11764

Mead, M. I., White, I. R., Nickless, G., Wang, K.-Y., & Shallcross, D. E. (2008). An estimation of the global emission of methyl bromide from rapeseed (*Brassica napus*) from 1961 to 2003. *Atmospheric Environment*, *42*(2), 337–345. https://doi.org/10.1016/j.atmosenv.2007.09.020

Miller, B. R., Huang, J., Weiss, R. F., Prinn, R. G., & Fraser, P. J. (1998). Atmospheric trend and lifetime of chlorodifluoromethane (HCFC-22) and the global tropospheric OH concentration. *Journal of Geophysical Research*, *103*, 13,237–13,248. https://doi.org/10.1029/98JD00771

NERRS: NOAA National Estuarine Research Reserve System (2016). System-wide monitoring program data accessed from the NOAA NERRS Centralized Data Management Office website. Retrieved from http://www.nerrsdata.org/

Pattey, E., Desjardins, R. L., & Rochette, P. (1993). Accuracy of the relaxed eddy-accumulation technique, evaluated using CO_2 flux measurements. *Boundary-Layer Meteorology*, *66*(4), 341–355. https://doi.org/10.1007/BF00712728

Pendleton, L., Donato, D. C., Murray, B. C., Crooks, S., Jenkins, W. A., Sifleet, S., et al. (2012). Estimating global "Blue Carbon" emissions from conversion and degradation of vegetated coastal ecosystems. *PLoS One*, *7*(9), e43542. https://doi.org/10.1371/journal.pone.0043542

Peterson, M. E., Daniel, R. M., Danson, M. J., & Eisenthal, R. (2007). The dependence of enzyme activity on temperature: Determination and validation of parameters. *Biochemical Journal*, *402*(2), 331–337. https://doi.org/10.1042/BJ20061143

Redeker, K. R., Andrews, J., Fischer, F., Sass, R., & Cicerone, R. J. (2002). Interfield and intrafield variability of methyl halide emissions from rice paddies. *Global Biogeochemical Cycles*, *16*(4), 1125. https://doi.org/10.1029/2002GB001874

Rhew, R., & Mazéas, O. (2010). Gross production exceeds gross consumption of methyl halides in northern California salt marshes. *Geophysical Research Letters*, *37*, L18813. https://doi.org/10.1029/2010GL044341

Rhew, R. C., Teh, Y. A., & Abel, T. (2007). Methyl halide and methane fluxes in the northern Alaskan coastal tundra. *Journal of Geophysical Research*, *112*, G02009. https://doi.org/10.1029/2006JG000314

Rhew, R. C., Deventer, M. J., Turnipseed, A. A., Warneke, C., Ortega, J., Shen, S., et al. (2017). Ethene, propene, butene and isoprene emissions from a ponderosa pine forest measured by relaxed eddy accumulation. *Atmospheric Chemistry and Physics*, *17*(21), 13,417–13,438. https://doi.org/10.5194/acp-17-13417-2017

Rhew, R. C., Miller, B. R., Bill, M., Goldstein, A. H., & Weiss, R. F. (2002). Environmental and biological controls on methyl halide emissions from southern California coastal salt marshes. *Biogeochemistry*, *60*, 141–161.

Rhew, R. C., Miller, B. R., & Weiss, R. F. (2000). Natural methyl bromide and methyl chloride emissions from coastal salt marshes. *Nature*, *403*(6767), 292–295. https://doi.org/10.1038/35002043

Rhew, R. C., Østergaard, L., Saltzman, E. S., & Yanofsky, M. F. (2003). Genetic control of methyl halide production in *Arabidopsis*. *Current Biology*, *13*(20), 1809–1813. https://doi.org/10.1016/j.cub.2003.09.055

Rhew, R. C., Whelan, M. E., & Min, D.-H. (2014). Large methyl halide emissions from South Texas salt marshes. *Biogeosciences*, *11*(22), 6427–6434. https://doi.org/10.5194/bg-11-6427-2014

Riederer, M., Hübner, J., Ruppert, J., Brand, W. A., & Foken, T. (2014). Application of relaxed eddy accumulation (REA) on managed grassland. *Atmospheric Measurement Techniques Discussions*, *7*(5), 4987–5026. https://doi.org/10.5194/amtd-7-4987-2014

Rubel, F., & Kottek, M. (2010). Observed and projected climate shifts 1901-2100 depicted by world maps of the Köppen-Geiger climate classification. *Meteorologische Zeitschrift*, *19*(2), 135–141. https://doi.org/10.1127/0941-2948/2010/0430

Saini, H. S., Attieh, J. M., & Hanson, a. D. (1995). Biosynthesis of halomethanes and methanethiol by higher plants via a novel methyltransferase reaction. *Plant, Cell & Environment*, *18*(9), 1027–1033. https://doi.org/10.1111/j.1365-3040.1995.tb00613.x

Saito, T., Yokouchi, Y., Kosugi, Y., Tani, M., Philip, E., & Okuda, T. (2008). Methyl chloride and isoprene emissions from tropical rain forest in Southeast Asia. *Geophysical Research Letters*, *35*, L19812. https://doi.org/10.1029/2008GL035241

Sharpe, P. J. H., & DeMichele, D. W. (1977). Reaction kinetics of poikilotherm development. *Journal of Theoretical Biology*, *64*(4), 649–670. https://doi.org/10.1016/0022-5193(77)90265-X

Simmonds, P. G., Derwent, R. G., Manning, A. J., Fraser, P. J., Krummel, P. B., O'Doherty, S., et al. (2004). AGAGE observations of methyl bromide and methyl chloride at Mace head, Ireland, and cape grim, Tasmania, 1998–2001. *Journal of Atmospheric Chemistry*, *47*(3), 243–269. https://doi.org/10.1023/B:JOCH.0000021136.52340.9c

Stemmler, I., Rothe, M., Hense, I., & Hepach, H. (2013). Numerical modelling of methyl iodide in the eastern tropical Atlantic. *Biogeosciences*, *10*(6), 4211–4225. https://doi.org/10.5194/bg-10-4211-2013

Thapar, N., Kim, A.-K., & Clarke, S. (2001). Distinct patterns of expression but similar biochemical properties of protein l-isoaspartyl methyltransferase in higher plants. *Plant Physiology*, *125*(2), 1023–1035. https://doi.org/10.1104/pp.125.2.1023

Tobias, V. D., Block, G., & Laca, E. A. (2016). Controlling perennial pepperweed (*Lepidium latifolium*) in a brackish tidal marsh. *Wetlands Ecology and Management*, *24*(4), 411–418. https://doi.org/10.1007/s11273-015-9464-9

USDA-ARS (2015). Germplasm esources Information Network (GRIN). Online Database Beltsville, Maryland, USA: National Germplasm Resources Laboratory. Retrieved from https://npgsweb.ars-grin.gov/gringlobal/Taxon/taxonomysearch.aspx

Villa, S. T., Xu, Q., Downie, A. B., & Clarke, S. G. (2006). *Arabidopsis* protein repair L-isoaspartyl methyltransferases: Predominant activities at lethal temperatures. *Physiologia Plantarum*, *128*(4), 581–592. https://doi.org/10.1111/j.1399-3054.2006.00772.x

Wang, J., Li, R., Guo, Y., Qin, P., & Sun, S. (2006). The flux of methyl chloride along an elevational gradient of a coastal salt marsh, Eastern China. *Atmospheric Environment*, *40*(34), 6592–6605. https://doi.org/10.1016/j.atmosenv.2006.05.065

Whitcraft, C. R., Grewell, B. J., & Baye, P. R. (2011). Estuarine vegetation at rush ranch open space preserve, san Franciso Bay National Estuarine Research Reserve, California. San Francisco Estuary and Watershed Science, 9(3). Retrieved from https://escholarship.org/uc/item/6j89531r

Woodwell, G. M., Rich, P. H., & Hall, C. A. S. (1973). The carbon cycle of estuaries. In G. M. Woodwell & E. V. Pecan (Eds.), *Carbon and the Biosphere, Proc. 24th Brookhaven Symposium in Biology, US Atomic Energy Commission Symp. Ser. CONF-720510* (pp. 221–240). Brookhaven, New York.

Wuosmaa, A. M., & Hager, L. P. (1990). Methyl chloride transferase: A carbocation route for biosynthesis of halometabolites. *Science*, *249*(4965), 160–162. https://doi.org/10.1126/science.2371563

Yokouchi, Y., Ikeda, M., Inuzuka, Y., & Yukawa, T. (2002). Strong emission of methyl chloride from tropical plants. *Nature*, *416*(6877), 163–165. https://doi.org/10.1038/416163a

Yokouchi, Y., Nojiri, Y., Toom-Sauntry, D., Fraser, P., Inuzuka, Y., Tanimoto, H., et al. (2012). Long-term variation of atmospheric methyl iodide and its link to global environmental change: Long-term change of methyl iodide. *Geophysical Research Letters*, *39*, L23805. https://doi.org/10.1029/2012GL053695

Yokouchi, Y., Saito, T., Ishigaki, C., & Aramoto, M. (2007). Identification of methyl chloride-emitting plants and atmospheric measurements on a subtropical island. *Chemosphere*, *69*(4), 549–553. https://doi.org/10.1016/j.chemosphere.2007.03.028